Water Research 220 (2022) 118689

Contents lists available at ScienceDirect

Water Research

journal homepage: www.elsevier.com/locate/watres

Microbial community mediates hydroxyl radical production in soil slurries by iron redox transformation

Dan Wan [a,b], Fei-Fei Liu [c], Jiu-Bin Chen [a], Andreas Kappler [d], Yakov Kuzyakov [e,f], Cong-Qiang Liu [a], Guang-Hui Yu [a,*]

[a] Institute of Surface-Earth System Science, School of Earth System Science, Tianjin University, Tianjin 300072, China
[b] School of Environmental Science and Engineering, Tiangong University, Tianjin 300387, China
[c] College of Resources and Environmental Sciences, Nanjing Agricultural University, Nanjing 210095, China
[d] Geomicrobiology, Center for Applied Geosciences, University of Tübingen, Tübingen 72076, Germany
[e] Department of Soil Science of Temperate Ecosystems, Department of Agricultural Soil Science, University of Göttingen, Göttingen 37073, Germany
[f] Agro-Technological Institute, Peoples Friendship University of Russia (RUDN University), Moscow 117198, Russia

ARTICLE INFO

Keywords:
Fenton reaction
Iron minerals
Microorganism-mineral interactions
Reactive oxygen species
Synergistic effect

ABSTRACT

The generation of reactive oxygen species (ROS) mediated by minerals and/or microorganisms plays a vital but underappreciated role in affecting carbon and nutrient cycles at soil-water interfaces. It is currently unknown which interactions between microbial communities and iron (Fe) minerals produce hydroxyl radical ($HO^{\bullet}$), which is the strongest oxidant among ROS. Using a series of well-controlled anoxic incubations of soil slurries, we demonstrated that interactions between microbial communities and Fe minerals synergistically drove $HO^{\bullet}$ production (up to ~100 nM after 21-day incubation). Microorganisms drove $HO^{\bullet}$ generation in anoxic environments predominantly by modulating iron redox transformation that was more prominent than direct production of ROS by microorganisms. Among the microbial communities, *Geobacter, Paucimonas, Rhodocyclaceae_K82*, and *Desulfotomaculum* were the key genera strongly affecting $HO^{\bullet}$ production. In manured soils, the former two species had higher abundances and were crucial for $HO^{\bullet}$ production. In contrast, the latter two species were mainly abundant and important in soils with mineral fertilizers. Our study suggests that abundant highly reactive oxidant $HO^{\bullet}$ can be generated in anoxic environments and the microbial community-mediated redox transformations of iron (oxyhydr)oxides may be responsible for the $HO^{\bullet}$ production. These findings shed light on the microbial generation of $HO^{\bullet}$ in fluctuating redox environments and on consequences for global C and nutrient cycling.

1. Introduction

The preservation and decomposition of soil organic carbon (SOC) has been the subject of scientific inquiry for decades, owing to its extremely vital role in regulating atmospheric CO_2 concentrations (Chenu et al., 2019; Lal, 2004; Paustian et al., 2016). Because of their large surface area and high adsorption affinity, Fe minerals are widely recognized as a rusty sink for C (Faust et al., 2021; Lalonde et al., 2012). However, Fe minerals may play a dualistic role in C transformations. Emerging evidence demonstrates that Fe mineral-driven hydroxyl radical ($HO^{\bullet}$) production plays a vital but underappreciated role in accelerating SOC decomposition in humid environments (Chen et al., 2020; Hall and Silver, 2013; Yu and Kuzyakov, 2021). As a nonselective and strong oxidant, $HO^{\bullet}$ radicals produced in some soils and ecosystems (e.g., desiccated and aqueous deserts, humid red soils in the tropics and wet subtropics, soils with fluctuating redox conditions) can drive 30% or even exceed 50% of total C losses (Georgiou et al., 2015; Wang et al., 2017a; Yu and Kuzyakov, 2021). The uncertain role of Fe minerals in SOC stabilization under fluctuating redox conditions has resulted in a huge challenge in achieving a better understanding of individual processes and consequences for global C cycling (Kleber et al., 2021; Yu and Kuzyakov, 2021).

The main pathways for $HO^{\bullet}$ production, driven by Fe minerals, in environments are classified as homogeneous Fenton reactions (Fe(II)/H_2O_2) and heterogeneous Fenton-like reactions (Du et al., 2021; Georgiou et al., 2015; Kappler et al., 2021; Melton et al., 2014; Page et al.,

* Corresponding author.
E-mail address: yuguanghui@tju.edu.cn (G.-H. Yu).

https://doi.org/10.1016/j.watres.2022.118689
Received 4 March 2022; Received in revised form 26 May 2022; Accepted 28 May 2022
Available online 29 May 2022

2013; Trusiak et al., 2018; Yu and Kuzyakov, 2021). During these reactions, the catalytic activity of Fe minerals is largely dependent on Fe redox chemistry and mineral surface reactivity (Chen et al., 2021; Chi et al., 2021, 2022a; Pereira et al., 2012; Yu and Kuzyakov, 2021; Yu et al., 2020). Such Fe minerals, e.g., goethite, haematite, lepidocrocite, ferrihydrite, and magnetite, coexist in environments and can be converted to one another under fluctuating redox conditions (Kappler and Straub, 2005; Weber et al., 2006a), making it difficult to identify their individual catalytic roles. Microorganisms are proposed to play an essential role in Fe redox cycling and the consequences of $HO^{\bullet}$ production in environments (Byrne et al., 2015; Du et al., 2020; Emerson et al., 2010; Kleber et al., 2021; Yu and Kuzyakov, 2021). Recent studies have observed $HO^{\bullet}$ production during the process of Fe mineral transformation, which is mediated by a single bacterial species (Du et al., 2019; Han et al., 2020; Wang et al., 2017b), confirming the essential role of microbially modulated Fe redox transformation in $HO^{\bullet}$ production. However, most bacteria do not exist as free-living individual species but as microbial communities, which are interconnected via the exchange of compounds, energy, and information to form complex interactions (e.g., competition, mutualism, and commensalism) (Flemming et al., 2016; Yuan et al., 2021). To date, the regulation of $HO^{\bullet}$ production driven by microbial communities and succession in the presence of Fe minerals remains poorly understood, hampering our understanding of soil C cycling mediated by biotic and abiotic processes.

This study aimed (i) to establish a link between microbial community composition, Fe redox transformation, and $HO^{\bullet}$ production, (ii) to assess the relative contribution of soil microbial communities to the production of $HO^{\bullet}$, and (iii) to identify the keystone bacterial species responsible for $HO^{\bullet}$ production. We hypothesized that microbial communities drive $HO^{\bullet}$ generation under anoxic conditions by (i) controlling the hydroxylation processes on the surface of iron minerals (Xian et al., 2019) and/or (ii) producing the trace amounts of oxygen by some microorganisms in the presence of electron donors (Kraft et al., 2022). To test our hypotheses, we first established a variety of microbial communities that were derived from topsoils (0–20 cm) from four long-term (26 years) fertilization treatments (Wen et al., 2018). This selection may also allow a better understanding of the formation of more reactive minerals and organo-mineral associations under organic fertilizations (Yu et al., 2017, 2020). Since soil organic matter (SOM) and minerals can interfere with ROS determination (Page et al., 2013; Yu and Kuzyakov, 2021), we used the soil slurries that contained only enriched microbial communities but removed most ROS quenchers (e.g., SOM and minerals) (Hori et al., 2010) in this study. We then conducted a series of sequential Fe (III) reduction and nitrate (NO_3^-)-dependent Fe(II) oxidation experiments by adding haematite, a model Fe(III)-bearing mineral with a ubiquitous distribution in ecosystems (Hochella et al., 2019; Schindler et al., 2019), to the soil slurries. Our results provide crucial insights into the mechanisms of microbial community-mediated $HO^{\bullet}$ generation in redox environments.

2. Materials and methods

2.1. Soil sampling

The long-term fertilization station was established on a Ferric Acrisol (WRB classification) in 1990 at Qiyang (26.75° N, 111.87° E), Hunan Province, China. Topsoil samples (0–20 cm) were collected in April 2016 from the following four treatments: (i) no fertilization (Control), (ii) swine manure fertilization (M), (ii) swine manure plus mineral nitrogen, phosphorus and potassium fertilization (MNPK), and (iv) mineral nitrogen, phosphorus and potassium fertilization (NPK). Each fertilization treatment had duplicate plots (200 m^2 per plot), which were completely randomly arranged in the field. More detailed information on the site is presented in Text S1 and previous publications (Wan et al., 2021; Wen et al., 2018; Yu et al., 2017, 2021). All plots were evenly separated into three regions, and 10 cores (diameter of 5 cm) from each region were randomly collected. Each sample was a composite of 30 random cores collected from a single plot. The fresh soil was air-dried, sieved (2 mm), and stored at 4 °C until further use. The basic soil properties are listed in Table S1.

2.2. Microbial community-Fe mineral incubation experiments

Before incubation, soil samples were thoroughly mixed and then partitioned into two subsamples: one was stored at 4 °C, and the second was sterilized by gamma radiation (3 kGy $hour^{-1}$ for 12 h) (Berns et al., 2008). Soil slurries were prepared by mixing the dry soil with sterile ultrapure water at a ratio of 1:1 (Hori et al., 2007). To allow for the activation of the soil microbes and the depletion of indigenous electron acceptors such as nitrate, sulfate, and Fe(III) minerals, slurries were pre-incubated under anoxic, dark conditions at 25 °C for 21 days (Ding et al., 2015; Hori et al., 2010). The pre-incubated soil slurries contained only enriched microbial communities but the most indigenous electron acceptors and ROS quenchers (e.g., SOM and minerals) were removed (Hori et al., 2010; Wen et al., 2018). After pre-incubation, the concentrations of Fe(II) and total dissolved Fe in the soil slurries were determined (Table S2). A basal PIPES-buffered artificial groundwater (AGW) medium (Table S3) supplemented with 11 mmol L^{-1} Na-acetate was used for the soil slurry enrichment culture experiment. The bottle of medium was inoculated with 1% (v/v) anoxic soil slurry immediately after collection and preparation as described above. The introduced concentrations of Fe(II) and total dissolved Fe by soil slurries in the medium are listed in Table S4.

In addition to slurry + haematite treatment (AGW medium amended with soil slurry and haematite), three control treatments were prepared to further verify the concerted effects of microbial communities and Fe redox transformation on the production of $HO^{\bullet}$: (i) only slurry addition (AGW medium amended with soil slurry); (ii) only haematite addition (AGW medium amended with haematite); and (iii) sterile slurry + haematite addition (AGW medium amended with sterilized soil slurry and haematite). Haematite (surface area, ca. 200 m^2 g^{-1}) (Fig. S1) was synthesized as previously described (Schwertmann and Cornell, 2008) and added at a final concentration of 25 mmol L^{-1}. All bottles were flushed with N_2 to remove the possible oxygen contamination and then sealed with butyl rubber septa, crimped with aluminum caps, wrapped with tin foil. All bottles were stored in an anaerobic glove box (LAB star, Braun, Germany) at room temperature without shaking during the whole incubation period. In total, each treatment was conducted in 66 replicates/bottles. The Fe(III) reduction stage lasted for ca. 21 days according to the measured Fe(II) concentrations, and then 0.3 mL of 1 mol L^{-1} $NaNO_3$ was re-added to the enrichment cultures (100 mL) to induce NO_3^--dependent Fe(II) oxidation (~21 days). Thus, the incubation period was separated into Fe(III) reduction and Fe(II) oxidation stages. During the Fe(III) reduction stage, haematite was the sole terminal electron acceptor, while acetate served as an electron donor. During the Fe(II) oxidation stage, NO_3^- and Fe(II) were the terminal electron acceptor and electron donor, respectively.

Subsamples were collected by the destructive sampling of a random triplicate setup at Days 0 and 1 and then every 2–5 days for analyses of NO_3^-, NO_2^-, NH_4^+, Fe(II), total dissolved Fe, bacterial community, and identity of Fe minerals. Three bottles were randomly selected from each treatment at Days 1, 8, 21, and 42 for $HO^{\bullet}$ analyses. The whole incubation and sampling process were carried out in the anaerobic glove box filled with 99.9% N_2 (25 ± 1 °C) to avoid oxygen contamination. A detailed schematic explaining the experimental design is shown in Fig. S2.

2.3. Chemical analyses

Soil pH was determined in a 1:2.5 ratio soil/water suspension. The total organic C and total nitrogen of soils were determined using a CN analyzer (VarioEL, Elementar GmbH, Germany) (Wan et al., 2019).

Total Fe in the soils was extracted by a mixture of concentrated acids (HNO_3, $HClO_4$, HCl, and HF), and the Fe in the extract was quantified by inductively coupled plasma-atomic emission spectrometry (5100, Agilent Technologies Inc., USA) (Wan et al., 2021). Soil nitrate (NO_3^-) and ammonium (NH_4^+) were extracted with 2 mol L^{-1} KCl and determined by a continuous flow analyzer (SAN++, Skalar, Holland) (Wen et al., 2018).

The concentrations of Fe(II) and total dissolved Fe (after reduction of Fe(III) with hydroxylamine-hydrochloride) in the slurry were measured using the *o*-phenanthroline colorimetric method (details in Text S2) (Ding et al., 2015; Wen et al., 2018). The NO_3^-, NO_2^-, and NH_4^+ concentrations were determined using a continuous flow analyzer (SAN++, Skalar, Holland). The $HO^•$ was trapped by terephthalic acid, and the fluorescent product, i.e., 2-hydroxyl terephthalic acid, was measured by ultra-performance liquid chromatography (details in Text S3) (Li et al., 2004). The identity of Fe minerals in the subsamples was analyzed by X-ray powder diffraction (XRD) and Fe K-edge extended X-ray absorption fine structure (EXAFS) spectroscopy; details are presented in Texts S4 and S5, respectively.

2.4. DNA extractions and microbial community sequencing

Soil slurry samples (0.5 g) at the initial stage, the end of the Fe(III) reduction stage and the end of the Fe(II) oxidation stage were used for DNA extraction with the MP FastDNA Spin Kit for soil (MP Biomedicals, USA) following the manufacturer's instructions. Three successive DNA extracts were pooled to reduce DNA extraction bias. Extracted DNA was stored at –80 °C before molecular analysis. The details of microbial community sequencing are shown in Text S6.

2.5. Statistical analyses

All statistical analyses were performed using R statistical software (version 4.1.0, https://www.r-project.org) and plots were produced using the "*ggplot2*" package (version 3.3.4, https://CRAN.R-project.org/package=ggplot2). The rarefaction curve and rank abundance curve were generated using the "*vegan*" (version 2.5.7, https://CRAN.R-project.org/package=vegan) and "*ggplot2*" packages, respectively. To determine the shared and unique OTUs between treatments, we constructed Venn diagrams using the "*VennDiagram*" package (version 1.6.20, https://CRAN.R-project.org/package=VennDiagram). To assess the microbial community diversity and richness, the Shannon and ACE indices were calculated using the "*vegan*" package. The Shannon and ACE indices are widely used to evaluate microbial community diversity and richness (Delgado-Baquerizo et al., 2016), with higher values suggesting higher diversity and richness. To test the bacterial diversity among fertilization treatments (β-diversity), nonmetric multidimensional scaling (NMDS, two axes) analysis and an ANOSIM test (analysis of similarities) based on unweighted UniFrac distance matrix were performed using the "*vegan*" package. The relationship between the bacterial community and geochemical variables was assessed by a Mantel test using the "*ggcor*" package (version 0.9.3.1, https://github.com/houyunhuang/ggcor) (details in Text S7). The significance ($p < 0.05$) of the Shannon index, ACE index, and $HO^•$ content between fertilization treatments was assessed using one-way ANOVA followed by Duncan's multiple range test using the "*agricolae*" package (version 1.3.3, https://CRAN.R-project.org/package=agricolae). The correlation among geochemical factors was tested using the "*ggcor*" package.

A classification random forest (RF) analysis (Montes et al., 2021) was used to identify the main predictors (i.e., microbial taxa) for Fe(II) and $HO^•$ production. The main aims of this analysis were to identify the potential microbial taxonomic predictors of $HO^•$ and to reduce the number of predictors for structural equation modeling (SEM). The RF analyses were performed using the "*randomForest*" package (version 4.6.14, https://CRAN.R-project.org/package=randomForest) (details in Text S8). We also applied a multiple regression model with variance decomposition analysis to confirm the RF analysis result by using the "*relaimpo*" package (version 2.2.5, https://CRAN.R-project.org/package=relaimpo). A heatmap was generated using the "*pheatmap*" package (version 1.0.12, https://CRAN.R-project.org/package=pheatmap) to assess the differences in potential microbial taxonomic predictor abundance among fertilizations. The correlations of the potential microbial taxonomic predictors of $HO^•$ with geochemical variables were tested using the "*ggcor*" package.

SEM was used to link the microbial community composition (i.e., the relative abundance of the main bacterial taxa) and iron to $HO^•$ production. This analysis helped us identify the main factor driving $HO^•$ production and explicitly evaluate the direct and indirect relationships between driving factors and $HO^•$ production. The SEM analysis was carried out using the "*lavaan*" package (version 0.6.9, https://CRAN.R-project.org/package=lavaan) (details in Text S9).

3. Results

3.1. Linking microbial mediated Fe redox cycling to $HO^•$ production in soil slurries

We observed a similar pattern of accumulation and consumption of Fe(II) and $HO^•$ in all haematite-treated soil slurries during the whole incubation (Fig. 1a and d). In the presence of haematite, Fe(II) was produced and increased in the soil slurries during the Fe(III) reduction stage. The increase in Fe(II) in the manured soil slurries (M and MNPK, by ca. 0.7 g L^{-1}) was higher than that in the soil with mineral fertilizers (NPK, by 0.5 g L^{-1}) or without fertilization (Control, by 0.4 g L^{-1}) (Fig. 1a). Accompanied by an increase in Fe(II), $HO^•$ was generated and gradually increased, and the accumulated amount of $HO^•$ in all soil slurries at the end of the Fe(III) reduction stage followed the order MNPK (94 nM) > M (91 nM) > NPK (82 nM) > Control (56 nM) (Fig. 1d). For the NO_3^--dependent Fe(II) oxidation stage, the introduction of NO_3^- at Day 21 resulted in rapid oxidation of Fe(II), with a faster oxidation rate observed in the manured soil slurries in the initial 10 days than that in the mineral fertilized or unfertilized soils (Fig. 1a and c). Similarly, a sharp decrease in the $HO^•$ amounts in all soil slurries at the Fe(II) oxidation stage revealed that Fe(II) dominated $HO^•$ generation (Fig. 1d). The addition of NO_3^- at Day 21 resulted in the rapid generation of NH_4^+ and NO_2^- (Fig. S3) in the soil slurries, with a higher rate observed in the manured soils, which was consistent with changes in the Fe(II) content (Fig. 1a). In addition, the total dissolved Fe concentrations in all soil slurries have similar patterns as total Fe(II) (Fig. 1b).

To further confirm the concerted effects of microbial communities and Fe redox transformation on $HO^•$ production, additional control experiments without the addition of microbial communities or haematite, i.e., with only haematite addition (no soil slurry), only slurry addition (no haematite), and soil sterilization (sterile soil slurry plus haematite), were conducted. A small increase in Fe(II) was observed in the slurry (by ca. 0.3 g L^{-1}, Fig. S4a) and sterilized (by ca. 0.2 g L^{-1}, Fig. S5b) soil slurries during the Fe(III) reduction stage. In the haematite-only addition treatment, the Fe(II) concentration was approximately 0.02 g L^{-1} during the whole incubation (Fig. S4d). A limited amount of $HO^•$ was detected in the slurry-only setups (< 20 nM, Fig. S4c), haematite-only setup (0 nM, Fig. S4f), and sterilized soil setups (ca. 6 nM, Fig. S5c) during the Fe(III) reduction stage, pointing to a strong linkage between $HO^•$ production and microbially mediated Fe redox cycling.

3.2. Transformation of Fe minerals

To investigate changes in the structure and mineralogy of haematite during microbially mediated Fe redox cycling, both XRD and Fe *K*-edge EXAFS were applied to identify the secondary Fe minerals in the soil slurries at the end of the Fe(III) reduction and Fe(II) oxidation stages. The XRD patterns of haematite strongly changed after incubation

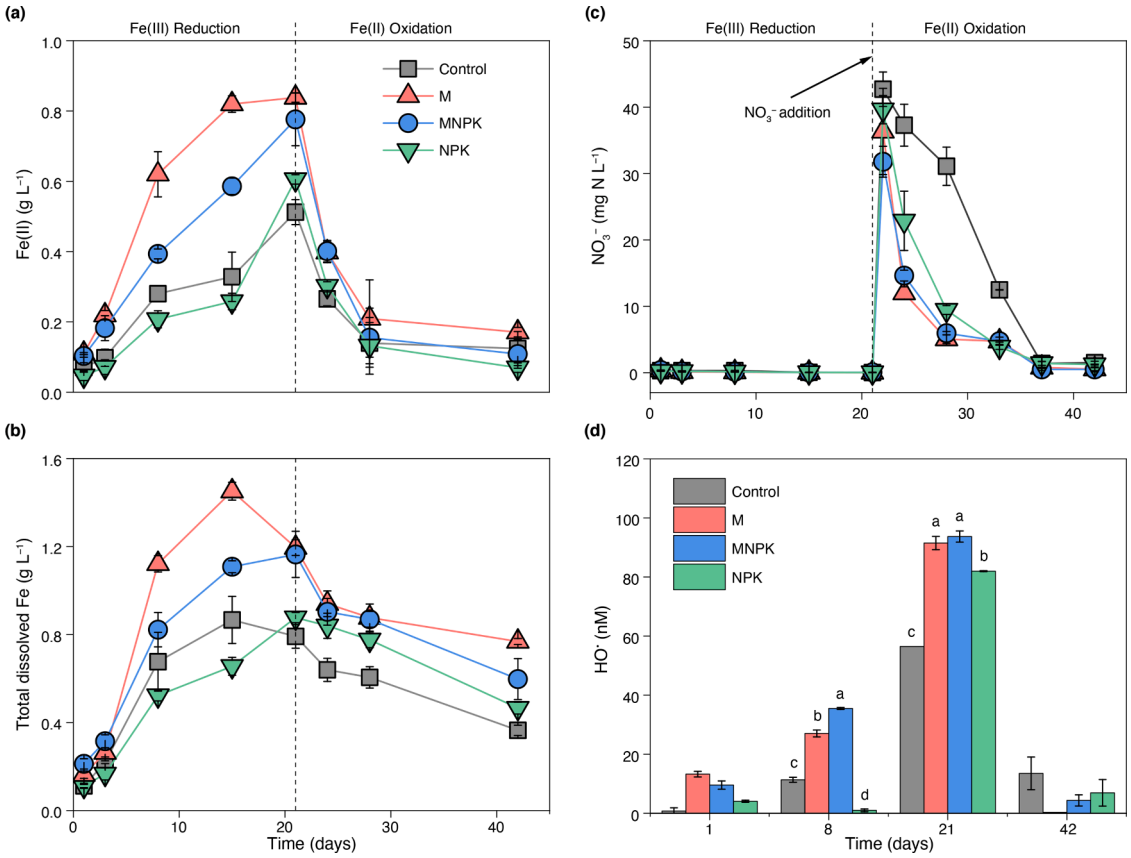

Fig. 1. Microbially mediated Fe redox cycling and HO• generation. Dynamics of (a) Fe(II), (b) total dissolved Fe, (c) NO_3^- and (d) HO• concentrations during the incubation experiments (slurry + haematite). NO_3^- as an electron acceptor was added at the end of the Fe(III) reduction stage. Significant differences in HO• concentrations among the treatments at the end of the Fe(III) reduction stage were determined using one-way ANOVA followed by Duncan's multiple range test at $p < 0.05$, in which the conditions of normality and homogeneity of variance were met. Letters above the bars denote a significant difference ($p < 0.05$) between fertilizations. Data are means ± SD ($n = 3$). Abbreviations: Control, no fertilization; M, swine manure fertilization; MNPK, swine manure plus mineral nitrogen, phosphorus and potassium fertilization; NPK, mineral nitrogen, phosphorus and potassium fertilization.

(Fig. S6), indicating that the haematite was transformed to other Fe-bearing minerals during microbially mediated Fe redox cycling. Goethite and ferrihydrite were identified by XRD in the M- and NPK-fertilized soil slurries, further supported by Fe *K*-edge EXAFS spectra (Fig. 2 and Table S5). Quartz was also identified in the soil slurries (Fig. S6).

To further quantify the composition of Fe minerals, we performed linear combination fitting (LCF) of the Fe k^3-weighted EXAFS spectra (Fig. 2 and Table S5). At the initial incubation stage, Fe-bearing minerals mainly consisted of haematite (91–97%). Intriguingly, at the end of the Fe(III) reduction stage, the highest percentage (25–27%) of haematite was converted to goethite and ferrihydrite in the manured soil slurries (i.e., M and MNPK), followed by ~23% in the unfertilized soil slurry (Control) and only 15% in the mineral fertilized soil slurry (NPK), pointing to the distinct microbial communities in the different fertilization soils. These newly formed Fe minerals may have higher chemical reactivities due to their nanometre particle sizes, amorphous and poorly crystalline structure, and more charged and rough surfaces than haematite. Notably, more crystalline forms (i.e., goethite) were found in the unfertilized and mineral fertilized soil slurries, while more poorly ordered phases (i.e., ferrihydrite) were formed in the manured soil slurries. At the end of the Fe(II) oxidation stage, the poorly ordered ferrihydrite increased in the unfertilized and mineral fertilized soil slurries.

3.3. Shifts in microbial communities and their linkage to Fe redox and HO• production

To disentangle the contribution of microbial communities to Fe redox reactions and HO• generation, we analyzed the microbial community composition in the initial soil slurries, after the Fe(III) reduction period, and after the Fe(II) oxidation period using Illumina MiSeq sequencing (optimized sequences and subsequently used sequences are listed in Table S6). The observed OTU counts (Table S7), OTU richness (ACE), and Shannon diversity (Fig. 3a and b) decreased with incubation duration, indicating that the increase in environmental stresses led to a drop in bacterial abundance and diversity. The Venn diagrams revealed that the shared bacterial numbers decreased with anoxic Fe incubations (Fig. S7), and manure-fertilized soils had a stronger capacity to conserve the shared bacterial groups than mineral-fertilized soils (Fig. S8). In particular, manured soil (i.e., M and MNPK) slurries had higher OTU counts, OTU richness, and Shannon diversity than mineral-fertilized soil (NPK) slurries during the whole incubation period. Shifts in microbial community composition were also supported by the dominant bacterial phyla (Fig. S9 and Text S12), rarefaction curves (Fig. S10), and rank abundance curves (Fig. S11). These results suggest a more robust microbial community structure in manured soils than in mineral-fertilized soil. A nonmetric multidimensional scaling (NMDS) plot showed that microbial communities had high clustering similarity between replicates but exhibited clear differences among the treatments (ANOSIM $r = 0.52$, $p = 0.001$, Fig. 3c).

A Mantel test was used to identify a possible correlation between the microbial community structures and HO• production (Fig. 3d). Bacterial

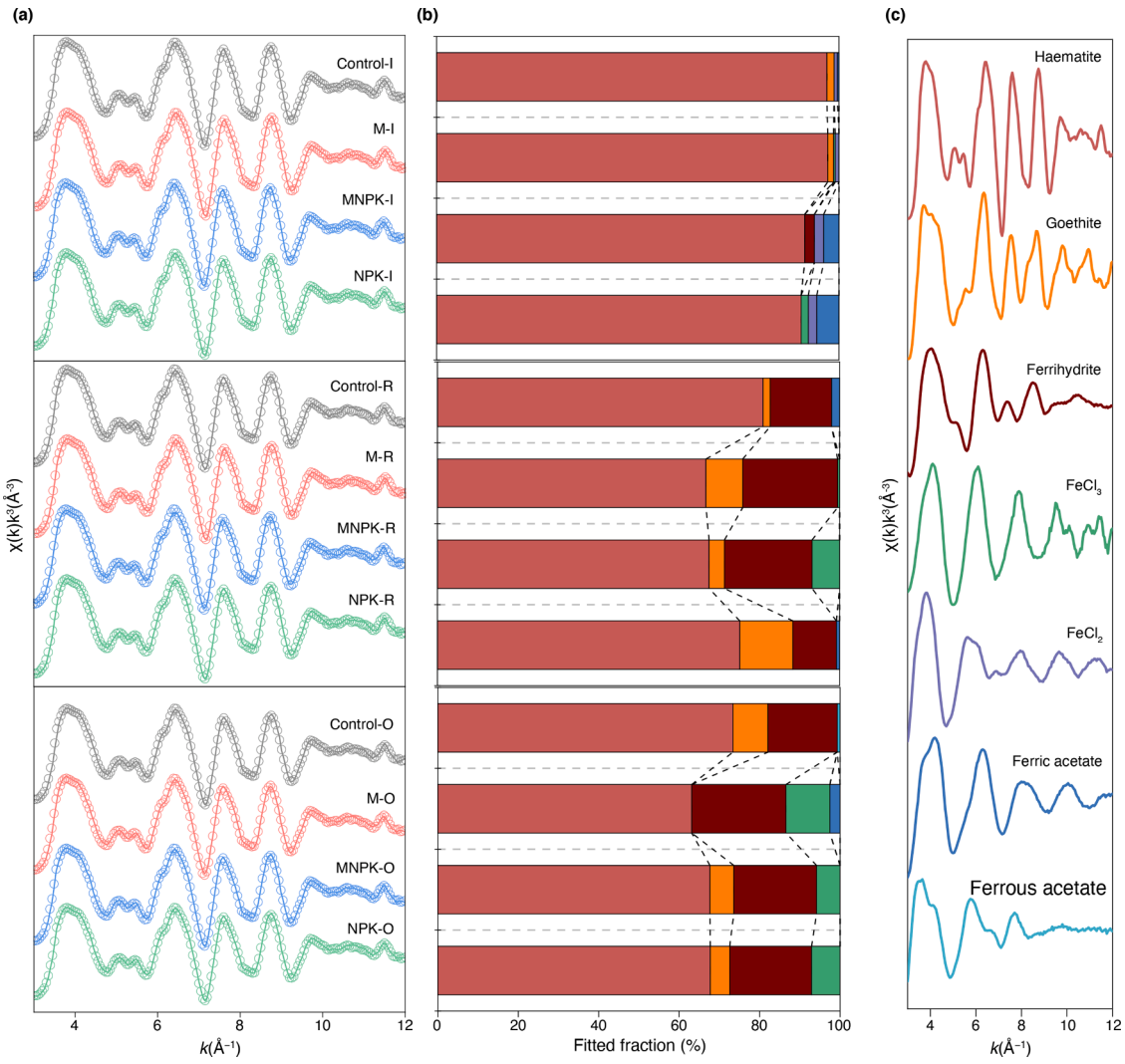

Fig. 2. EXAFS showing the transformation of Fe minerals during microbially mediated Fe redox cycling. (a) Fe k^3-weighted EXAFS spectra of samples at the initial soil slurry (-I), the end of the Fe(III) reduction stage (-R), and the end of the Fe(II) oxidation stage (-O). (b) Fe mineral fractions based on the LCF fitting of EXAFS spectra (also see the data in Table S5). (c) k^3-weighted EXAFS spectra of the Fe reference compounds used in the LCF fitting. Abbreviations: Control, no fertilization; M, swine manure fertilization; MNPK, swine manure plus mineral nitrogen, phosphorus and potassium fertilization; NPK, mineral nitrogen, phosphorus and potassium fertilization.

communities were closely correlated with $HO^{\bullet}$ concentrations, revealing that $HO^{\bullet}$ production may be strongly interlinked with microbial communities. However, bacterial communities and $HO^{\bullet}$ concentrations were significantly correlated with Fe(II), NO_3^-, pH, goethite, ferrihydrite, and haematite (Fig. 3d). Therefore, a partial Mantel test was used to further investigate the relationship between $HO^{\bullet}$ and bacterial community structures (Table S8). Indeed, $HO^{\bullet}$ had no significant relationship with bacterial community structures after the effect of Fe(II) was accounted for ($r = 0.09, p = 0.117$), implying that the microbial community may be indirectly linked with $HO^{\bullet}$ through Fe(II).

3.4. Potential microbial drivers of Fe(ii) and $HO^{\bullet}$ production

To identify the biological contribution of the dominant microbial genus to Fe(II) and $HO^{\bullet}$ production, RF analysis was used (Fig. 4). RF analysis screened only three and four microbial genera as predictors for Fe(II) ($R^2 = 0.74$, $p < 0.001$) and $HO^{\bullet}$ ($R^2 = 0.80$, $p < 0.001$), respectively. *K82*, belonging to the family *Rhodocyclaceae*, was the most important for predicting Fe(II) ($p < 0.01$) and $HO^{\bullet}$ ($p < 0.01$). Other important genera were (i) dissimilatory Fe(III)-reducing *Geobacter* (Lovley, 2006; Weber et al., 2006b), for Fe(II) ($p < 0.01$) and $HO^{\bullet}$ ($p < 0.01$); (ii) *Paucimonas* (family of *Burkholderiaceae*), characterized by rapid growth and rapid adaptation to mineralize soluble C (Jeewani et al., 2020) or Fe(II)-oxidizing ability (Peng et al., 2019), for Fe(II) ($p < 0.05$) and $HO^{\bullet}$ ($p < 0.01$); and (iii) dissimilatory Fe(III)-reducing *Desulfotomaculu* (Weber et al., 2006a), for $HO^{\bullet}$ ($p < 0.05$). These contributions were further supported by multivariate regression analysis (Tables S9 and S10). The relative abundance of the potential microbial taxonomic predictors in the soil slurries was illustrated by a heatmap, showing higher abundances of these microbes in the soil slurries at the end of the Fe(III) reduction stage (Fig. 4c). Interestingly, the potential microbial taxonomic predictors presented diverse abundances in different fertilized soil slurries at the end of the Fe(III) reduction stage. *Geobacter* and *Paucimonas* showed higher abundances in manured soil slurries, while *K82* and *Desulfotomaculum* showed higher abundances in mineral fertilized soil slurries independent of the addition of manure (i.e., MNPK and NPK).

3.5. Structural equation model linking microbial and iron to $HO^{\bullet}$ production

SEM was used for an in-depth analysis of the direct and indirect

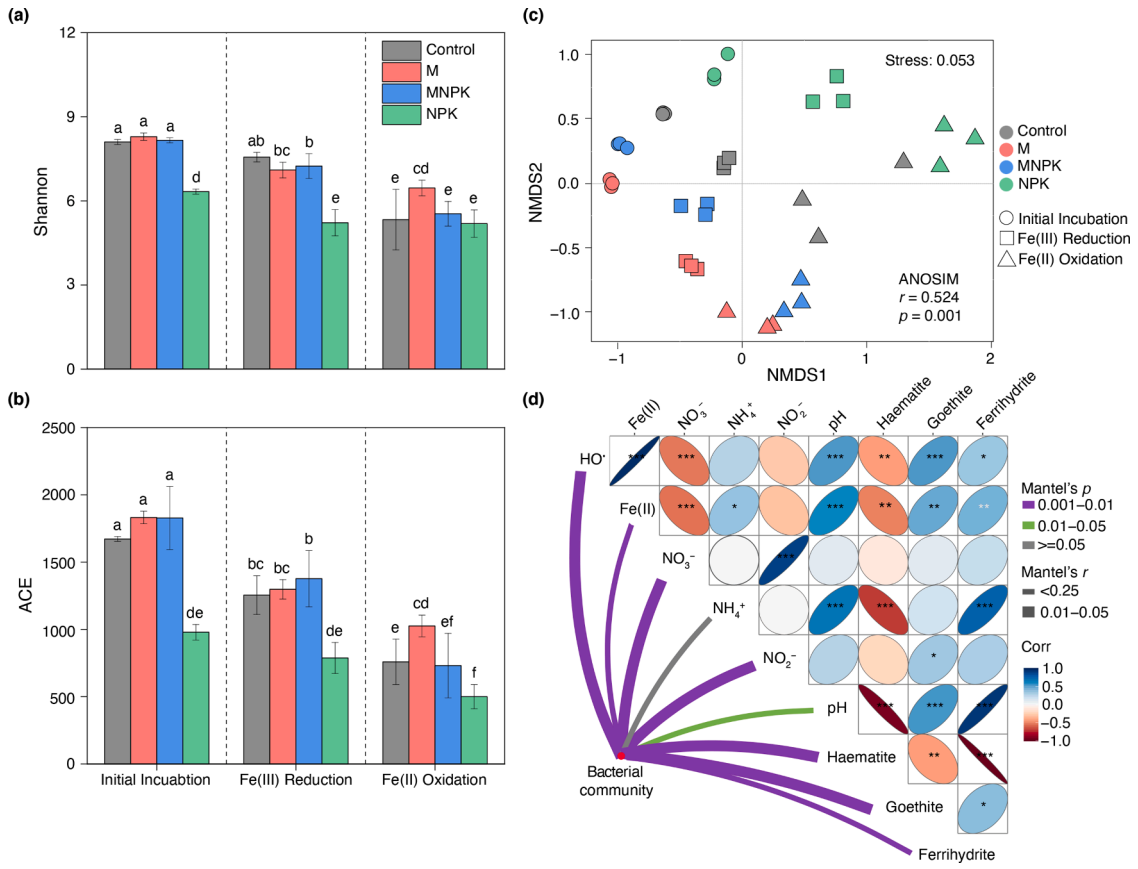

Fig. 3. Shifts in bacterial community diversity and the relationships between geochemical variables and bacterial communities. Column plots illustrate variation in bacterial community (a) diversity and (b) richness. Statistical differences between the fertilizations were determined using one-way ANOVA followed by Duncan's multiple range test at $p < 0.05$, in which the conditions of normality and homogeneity of variance were met. Letters show significant differences between the fertilizations ($p < 0.05$). (c) Non-metric multidimensional scaling (NMDS) plot shows the whole-community similarity among treatments and sample replicates. NMDS plot derived from UniFrac distance analysis of OTU composition based on unweighted (qualitative) comparisons. Colours correspond to fertilizations and shapes to incubation stages. Similarity values among the samples are examined via the ANOSIM test, which is shown in the plot. (d) Correlations of the microbial community structures (Bray–Curtis distance) with geochemical variables. Edge width corresponds to Mantel's *r* value, and the edge color denotes statistical significance. Pairwise correlations of geochemical variables are shown with a color gradient denoting Pearson's correlation coefficient. Abbreviations: Control, no fertilization; M, swine manure fertilization; MNPK, swine manure plus mineral nitrogen, phosphorus and potassium fertilization; NPK, mineral nitrogen, phosphorus and potassium fertilization.

effects of microbial drivers on HO• production. The SEM explained 98.0% of the variation in HO• production and provided a good fit using the χ^2 test, RMSEA, CFI, and Bollen-Stine bootstrap metrics (Fig. 5a) (Grace, 2006; Schermelleh-Engel et al., 2003). The model confirmed the importance of microbial drivers in HO• production, with the importance (based on the total standardized coefficient) following the order *Rhodocyclaceae_K82* > *Desulfotomaculum* > *Paucimonas* > *Geobacter* (Fig. 5b). Specifically, our SEM analysis suggested that *Rhodocyclaceae_K82*, and *Desulfotomaculum* abundances and Fe(II) and newly formed Fe mineral (i.e., ferrihydrite plus goethite) contents had direct positive effects on HO• production (Fig. 5b). Most importantly, our SEM analysis demonstrated that *Geobacter, Rhodocyclaceae_K82, Desulfotomaculum*, and *Paucimonas* indirectly regulate HO• production via a positive association with Fe(II) (Fig. 5). Furthermore, compared with the standardized path coefficients for HO• production, the indirect effects of *Geobacter, Desulfotomaculum, Rhodocyclaceae_K82*, and *Paucimonas* (ranging from 0.18 to 0.45), were much stronger than their direct effects (0.00 to 0.14; Fig. 5b). Taken together, SEM analysis explained most of the variation in the contents of HO•, which is mainly indirectly driven by the microbial community structures through the regulating of Fe redox cycling.

4. Discussion

4.1. Effects of long-term fertilizations on microbial communities and Fe transformation

High clustering similarity between replicates but significant differences among the soils (Fig. 3c) revealed that long-term fertilization strongly shifted the soil microbial community composition, which was consistent with previous observations in red soils (Luo et al., 2020; Wen et al., 2018; Xun et al., 2016). We showed that long-term (26 years) manure-fertilized soils (i.e., M and MNPK) had higher OTU counts and microbial diversity than mineral-fertilized soils (NPK) during the reduction period (Fig. 3a, b, and Table S7). This is in line with changes in Fe(II) (Fig. 1a) and newly formed minerals (Fig. 2). During anoxic incubation, haematite, as the most stable Fe(III) oxide, may be transformed to highly reactive ferrihydrite and goethite either (i) via Fe(III) reduction followed by surface-dependent Fe(II) oxidation or (ii) through dissolution and reprecipitation processes (Qafoku et al., 2020; Raiswell, 2011; Shi et al., 2009).

4.2. Interactions between key microbial groups (taxa) with the Fe(ii) and HO• production in anoxic soil slurries

Random forest, multiple regression model, and SEM analyses showed

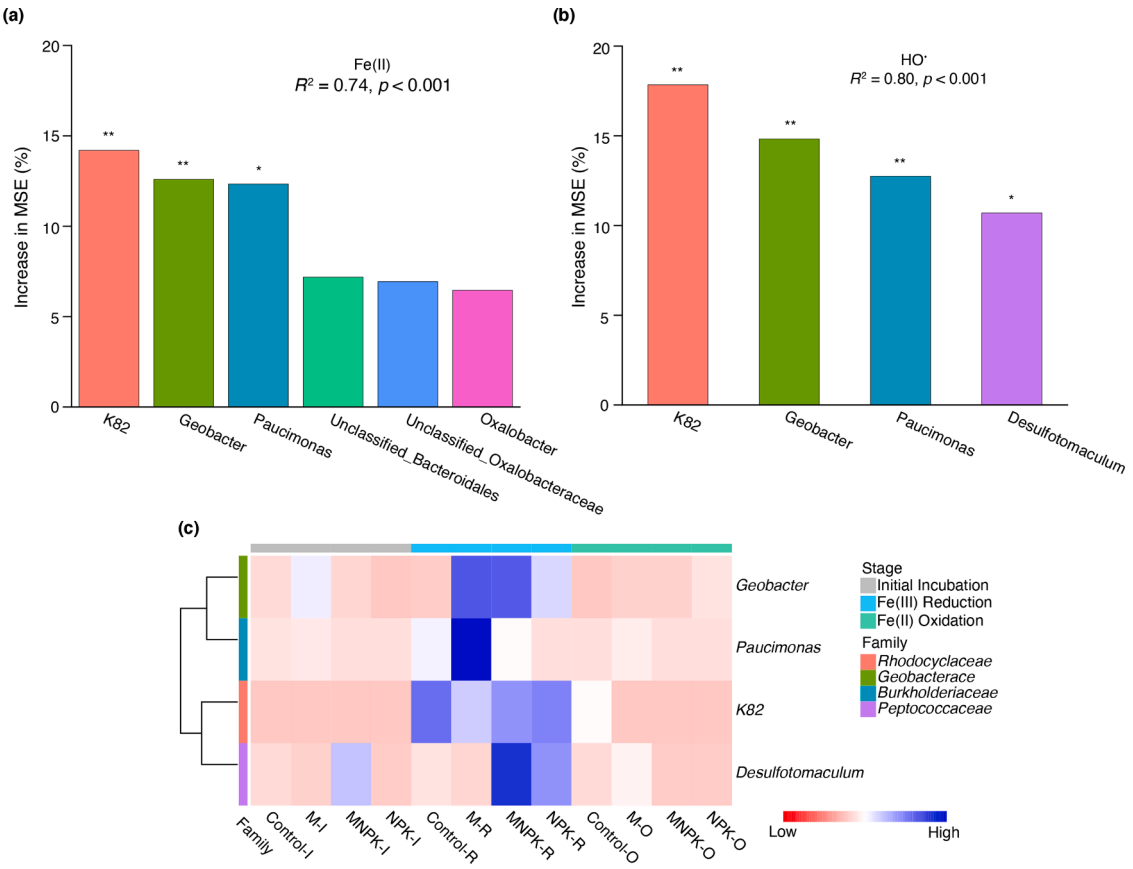

Fig. 4. Potential microbial taxonomic predictors of Fe(II) and HO• production. Random forest (RF) mean predictor importance (percentage of increase of mean square error) of microbial genera as drivers for (a) Fe(II) and (b) HO• production. The accuracy importance measure was computed for each tree and averaged over the forest (5000 trees). Percentage increases in the MSE (mean squared error) of variables were used to estimate the importance of these predictors, and higher MSE% values imply more important predictors. Significance levels are as follows: *$p < 0.05$ and **$p < 0.01$. (c) Heatmap showing the relative abundances of potential microbial taxonomic predictors in the soil slurries depending on fertilization and reduction (-R) or oxidation (-O) stages. Abbreviations: Control, no fertilization; M, swine manure fertilization; MNPK, swine manure plus mineral nitrogen, phosphorus and potassium fertilization; NPK, mineral nitrogen, phosphorus and potassium fertilization.

that the Fe(II) production was directly and significantly regulated by the abundance of *Rhodocyclaceae_K82, Geobacter, Paucimonas*, and *Desulfotomaculum* (Figs. 4a, 5a, S12 and Table S9), pointing out that these four bacterial genera may act as the keystone Fe-reducing microorganisms in the anoxic soil slurries. Both *Geobacter* and *Desulfotomaculum* are widely recognized Fe(III)-reducing microorganisms under anoxic conditions (Weber et al., 2006a). Regarding the genus *K82*, the family *Rhodocyclaceae* has been revealed to participate in Fe(III) reduction (Porsch et al., 2009). Since acetate was the sole terminal electron donor at the Fe (III) reduction stage, we speculate that the genus *K82* participated in Fe (III) reduction. Acetate may be rapidly utilized by microorganisms from soil within few hours (Fischer and Kuzyakov, 2010; Qiu et al., 2017). A strongly positive correlation between *K82* and Fe(II) further confirmed this speculation (Fig. S13). The genus *Paucimonas* increased with Fe(II) concentration (Fig. S13) and showed higher relative abundance in the soils at the Fe(III) reduction stage (Fig. 4c). Similarly, the genus *Paucimonas* participated in soil N and Fe cycles (Peng et al., 2019). Therefore, we assume that *Paucimonas* may be involved in Fe(III) reduction with haematite as the sole electron acceptor at the reduction stage.

Similar to Fe(II), our findings also demonstrated that the HO• production was closely linked to the keystone genera *K82, Geobacter, Paucimonas*, and *Desulfotomaculum* (Figs. 4b, 5, and Table S10). We further found small but significant direct control of HO• production by *K82* ($p < 0.001$) and *Desulfotomaculum* ($p < 0.001$) (Fig. 5a). Some keystone genera have the ability to produce trace O_2 in anoxic environments (Kraft et al., 2022). The produced trace O_2 with acetate as the electron donor can be further converted to extracellular $O_2^{\bullet-}$ and H_2O_2 (the precursor to HO• formation) through enzymatic catalysis (Diaz et al., 2013; Gordon et al., 1953; Learman et al., 2011; Lieberman and Barker, 1954). Moreover, $O_2^{\bullet-}$ can react with H_2O_2 to form HO• (Hayyan et al., 2016) through the Haber-Weiss reaction (Haber et al., 1934). The secretion of $O_2^{\bullet-}$ and the reduction of Fe(III) are reported to connect with microbial oxidative stress removal and iron acquisition (Yu et al., 2020). Hence, we assume that the direct control exerted by *K82* and *Desulfotomaculum* on HO• production may occur by regulating microbial mediated $O_2^{\bullet-}$ formation.

Intriguingly, *K82, Geobacter, Paucimonas*, and *Desulfotomaculum* also control HO• production through an indirect pathway (Fig. 5b). This is not surprising, as Fe(II) is involved in catalyzing HO• generation (Garrido-Ramírez et al., 2010; Georgiou et al., 2015; Page et al., 2013; Pereira et al., 2012; Petigara et al., 2002; Trusiak et al., 2018; Yu and Kuzyakov, 2021), and the Fe(II) production in our study was directly and significantly ($p < 0.05$) regulated by *K82, Geobacter, Paucimonas*, and *Desulfotomaculum* (Figs. 5a and S12). Compared to other soil slurries, a higher abundance of *Geobacter* and *Paucimonas* (Fig. 4c) in the manure-fertilized soil slurries resulted in much more HO• production (Fig. 1d), implying the importance of fertilization treatments in modulating HO• production and its key drivers. Taken together, these results indicated that microbial communities may drive HO• production through mediating both the extracellular $O_2^{\bullet-}$ formation and Fe redox cycling. Indeed, the stronger indirect impact of *Geobacter, Desulfotomaculum, K82*, and *Paucimonas* on HO• formation (Fig. 5b) suggests that

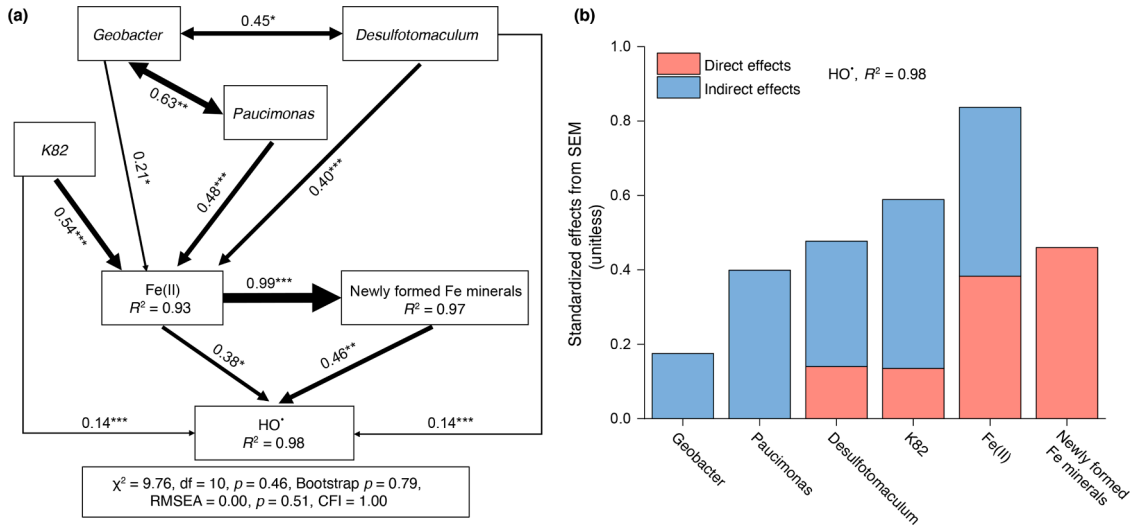

Fig. 5. SEM showing the relationships of potential microbial taxonomic predictors of HO• (derived from RF analysis) and iron (Fe(II) and the newly formed iron minerals) on HO• production. (a) SEM describing the effects of the potential microbial taxonomic predictors of HO• (derived from RF analysis), Fe(II), and newly formed Fe minerals (goethite and ferrihydrite) on HO• concentrations. Numbers adjacent to arrows are standardized path coefficients, analogous to partial regression weights and indicative of the effect size of the relationship. Black and red arrows represent significant positive and negative relationships, respectively. The arrow width is proportional to the strength of the path coefficients. As in other linear models, R^2 denotes the proportion of variance explained and appears below every response variable in the model. Model fitness details (χ^2, p, RMSEA, nonparametric bootstrap parameters, and CFI are close by figure) are close to figure. The significance levels of each predictor are as follows: $^*p < 0.05$, $^{**}p < 0.01$, and $^{***}p < 0.001$. (b) Standardized effects derived from the SEM. The panel represents standardized direct and indirect effects making together to total effects from each variable on HO• production.

microbial communities control HO• generation in an anaerobic environment primarily through mediating Fe redox cycling. These results provide direct evidence for the microbial mediation of Fe redox cycling linked to HO• production in anoxic environments.

Furthermore, the production of HO• radicals causes cell inactivation or inhibits the growth of cells through triggering membrane lipid peroxidation (Wang et al., 2017; Zhang et al., 2020). During the Fe(III) reduction stage, decrease in the observed OTU counts (Table S7), OTU richness (ACE), and Shannon diversity may be a result of the production of HO• (Fig. 3a and b). Consequently, the production of HO• radicals alters the activity and composition of microbial communities, possibly through a damage of membrane lipid peroxidation. The selective pressure of HO• radicals on microbial communities further affected Fe species transformation (Fig. 3d).

4.3. Possible mechanisms of HO• generation under anoxic environments

HO• radicals can be produced via photochemical (Georgiou et al., 2015; Page et al., 2013; Kappler et al., 2021), biotic (Han et al., 2020; Zhang et al., 2020; Kappler et al., 2021), or abiotic (Garrido-Ramírez et al., 2010; Kappler et al., 2021) pathways. Yet, it remains unclear how HO• can be produced under anoxic environments. Recently, Xian et al. (2019) showed that interactions between mineral defect sites of Fe (oxyhydr)oxides and H_2O in anoxic environments made the hydroxylation energetically favorable on the surface of iron minerals (Eq. (1)).

$$\equiv \mathrm{Fe(III)} + \mathrm{H_2O} \rightarrow \equiv \mathrm{Fe(II)} + \mathrm{HO^\bullet} + \mathrm{H^+} \quad (1)$$

This finding provides new insight into iron mineral-assisted HO• formation in anoxic conditions. Moreover, Kraft et al. (2022) proposed the following oxygen production pathway in *Nitrosopumilus maritimus* (Eq. (2)):

$$4\mathrm{NO_2^-} + 4\mathrm{e^-} \rightarrow 4\mathrm{NO} + \mathrm{O_2} + 2\mathrm{N_2O} \quad (2)$$

This pathway requires electrons to produce O_2, which may partly be supplied by acetate in our study. In the presence of O_2 traces, HO• radicals can be further produced by microbial modulation of iron redox transformation via Fenton or Fenton-like reactions (Kappler et al., 2021; Yu and Kuzyakov, 2021). Our SEM results (Fig. 5) showed that microorganisms drove HO• generation in anoxic environments predominantly by modulation of iron redox transformation that was more prominent than microbial direct roles. Therefore, the HO• in anoxic environments may be mainly generated through abiotic (Eq. (1)) rather than biotic (Eq. (2)) processes, which needs further exploration.

4.4. Environmental implications

The oxidation of Fe(II) or Fe(II)-bearing minerals in aerobic environments is the vital source of intensive ROS fluxes at soil-water interfaces (Chen et al., 2021; Chi et al., 2022b; Du et al., 2021; Georgiou et al., 2008; Han et al., 2021; Melton et al., 2014; Op De Beeck et al., 2018; Schoonen et al., 2006). In anoxic soil slurries, the cumulative amounts of HO• were less than 100 nM (Fig. 1d), which were 2–4 orders of magnitude lower than those in the oxygenation processes of surface sediments (Tong et al., 2016) or anoxic-oxic cycles of sediments (Han et al., 2020; Zhang et al., 2020). Although the HO• amounts produced in anoxic environments are low (Fig. 1d), it is very important to close a loop of the HO• production in both anoxic and oxic environments. These findings imply that (1) HO• can be sustainably generated in natural ecosystems and (2) anoxic environments may be a new HO• source.

The low HO• production in anoxic environments may possess a limited impact on C emission but a profound impact on soil C persistence (Faust et al., 2021; Lehmann et al., 2020). In humid soils, however, the ROS-mediated SOC decomposition counteracts C protection by minerals (Chen et al., 2020). Fe minerals and microbial communities synergistically increased CO_2 efflux up to ~15 times accompanied by a burst of HO• in the presence of plant residues (Du et al., 2020), pointing to the critical role of ROS production in elucidating the mechanisms of "priming effects" in soil "hotspots" (e.g., soil-water interfaces) (Kuzyakov et al., 2000; Merino et al., 2020). Moreover, the HO• burst is important for the bioavailability of the N pool in soils (Op De Beeck et al., 2018; Wang et al., 2021). On the other hand, the generated HO• can easily split chemical bonds in SOC, resulting in an increase in dissolved OC release and OC bioavailability (Du et al., 2020). Both charged small molecules and water-soluble macromolecules are favorable for binding on mineral surfaces and then form newly organo-mineral

complexes to increase the persistence of C in soils (Faust et al., 2021; Lehmann et al., 2020; Kleber et al., 2005; Kögel-Knabner et al., 2008). Although ROS species have a very short lifespan (Yu and Kuzyakov, 2021) at soil-water interfaces, microbial chelator-mediated Fenton catalysis can promote sustained ROS generation (Tamaru et al., 2019), which may have a profound impact on C and nutrient cycles in certain ecosystems (e.g., flooded soils, humid forest, or lake sediments). Our finding also indicated that organic inputs (e.g., manure) strongly increased the $HO^{\bullet}$ concentrations when compared to unfertilized control or soil with solely mineral fertilization. Consequently, this explains the higher mineral-associated C content in soils with organic fertilization (Yu et al., 2017).

More broadly, weather extremes (e.g., extreme precipitation or drought events) as well as climatic trends (e.g., stratospheric ozone depletion) may impart soil slurries with stronger redox fluctuations and UV and thus more ROS production (Overland et al., 2016; Smith et al., 2017; Sulzberger et al., 2019), which will definitely elevate the role of ROS in C and nutrient cycles in some ecosystems (e.g., humid forests or dry deserts). Therefore, in a changing world, we call for studying complex environmental gradients, long-term time series, and modeling to establish causality between interconnected community interactions (e.g., competition, mutualism, and commensalism) and redox-active minerals and their linkage to C and nutrient cycling in water ecosystems.

4. Conclusions and future perspectives

Our findings showed that interactions between microbial communities and Fe minerals in soil slurries synergistically drive $HO^{\bullet}$ production through microbial Fe(III) reduction and transformation to newly formed minerals. These microbially mediated Fe(III) reduction and transformation to new minerals were predominantly responsible for $HO^{\bullet}$ production in the anoxic environment. $HO^{\bullet}$ production was closely linked to the keystone genera *K82, Geobacter, Paucimonas*, and *Desulfotomaculum*. The discrepancies in the abundance of these genera interpreted well the $HO^{\bullet}$ production in soil slurries under a wide range of fertilization practices. Because microorganisms in soil are present but frequently not active (Blagodatskaya and Kuzyakov, 2013; Hori et al., 2010), further investigations should focus on the functions of the active microbial genera (i.e., *Geobacter, Desulfotomaculum, K82*, and *Paucimonas*) producing $HO^{\bullet}$. Stable isotope probing and pyrosequencing techniques seem very promising to link the microbial activities with the functions specific for $HO^{\bullet}$ production (Ding et al., 2015; Hori et al., 2010). Altogether, our findings establish a causality between $HO^{\bullet}$ production and microbial-mineral interactions at soil-water interfaces, and show the profound impact on carbon and nutrient cycles in anoxic environments.

Declaration of Competing Interest

The authors declare that they have no known competing financial interests or personal relationships that could have appeared to influence the work reported in this paper.

Data availability

The raw sequence data of this study are deposited in the NCBI Sequence Read Archive (BioProject accession number PRJNA756141).

Acknowledgments

This work was funded by the National Natural Science Foundation of China (41977271 and 42003010) and China Postdoctoral Science Foundation (2019M661028 and 2021T140507). The publication was supported by the "RUDN University Strategic Academic Leadership program". The authors thank the staff for their support at the BL14W beamline at Shanghai Synchrotron Radiation Facility (SSRF), for assistance during data collection. We thank Dr. Xuesong Luo (College of Resources and Environment, Huazhong Agricultural University, China) and Dr. Jiakai Liu (School of Environment, Beijing Normal University, China) for their help in statistical analyses.

Supplementary materials

Supplementary material associated with this article can be found, in the online version, at doi:10.1016/j.watres.2022.118689.

References

Berns, A.E., Philipp, H., Narres, H.D., Burauel, P., Vereecken, H., Tappe, W., 2008. Effect of gamma-sterilization and autoclaving on soil organic matter structure as studied by solid state NMR, UV and fluorescence spectroscopy. Eur. J. Soil Sci. 59 (3), 540–550.
Blagodatskaya, E., Kuzyakov, Y., 2013. Active microorganisms in soil: critical review of estimation criteria and approaches. Soil Biol. Biochem. 67, 192–211.
Byrne, J.M., Klueglein, N., Pearce, C., Rosso, K.M., Appel, E., Kappler, A., 2015. Redox cycling of Fe(II) and Fe(III) in magnetite by Fe-metabolizing bacteria. Science 347 (6229), 1473–1476.
Chen, C.M., Hall, S.J., Coward, E., Thompson, A., 2020. Iron-mediated organic matter decomposition in humid soils can counteract protection. Nat. Commun. 11 (1), 2255.
Chen, N., Huang, D.Y., Liu, G.X., Chu, L.G., Fang, G.D., Zhu, C.Y., Zhou, D.M., Gao, J., 2021. Active iron species driven hydroxyl radicals formation in oxygenation of different paddy soils: implications to polycyclic aromatic hydrocarbons degradation. Water Res. 203, 117484.
Chenu, C., Angers, D.A., Barré, P., Derrien, D., Arrouays, D., Balesdent, J., 2019. Increasing organic stocks in agricultural soils: knowledge gaps and potential innovations. Soil Tillage Res. 188, 41–52.
Chi, Z.L., Yu, G.H., Kappler, A., Liu, C.Q., Gadd, G.M., 2022a. Fungal-mineral interactions modulating intrinsic peroxidase-like activity of iron nanoparticles: implications for the biogeochemical cycles of nutrient elements and attenuation of contaminants. Environ. Sci. Technol. 56 (1), 672–680.
Chi, Z.L., Yu, G.H., Teng, H.H., Liu, H.G., Wang, J., Liu, C.Q., Shen, Q.R., Gadd, G.M., 2022b. Molecular trade-offs between lattice oxygen and oxygen vacancy drive organic pollutant degradation in fungal biomineralized exoskeletons. Environ. Sci. Technol. https://doi.org/10.1021/acs.est.2c01388.
Chi, Z.L., Zhao, X.Y., Chen, Y.L., Hao, J.L., Yu, G.H., Goodman, B.A., Gadd, G.M., 2021. Intrinsic enzyme-like activity of magnetite particles is enhanced by cultivation with *Trichoderma guizhouense*. Environ. Microbiol. 23 (2), 893–907.
Delgado-Baquerizo, M., Maestre, F.T., Reich, P.B., Jeffries, T.C., Gaitan, J.J., Encinar, D., Berdugo, M., Campbell, C.D., Singh, B.K., 2016. Microbial diversity drives multifunctionality in terrestrial ecosystems. Nat. Commun. 7 (1), 10541.
Diaz, J.M., Hansel, C.M., Voelker, B.M., Mendes, C.M., Andeer, P.F., Zhang, T., 2013. Widespread production of extracellular superoxide by heterotrophic bacteria. Science 340 (6137), 1223–1226.
Ding, L.J., Su, J.Q., Xu, H.J., Jia, Z.J., Zhu, Y.G., 2015. Long-term nitrogen fertilization of paddy soil shifts iron-reducing microbial community revealed by RNA-^{13}C-acetate probing coupled with pyrosequencing. ISME J. 9 (3), 721–734.
Du, H.Y., Cao, Y.X., Li, Z., Li, L.N., Xu, H.C., 2021. Formation and mechanisms of hydroxyl radicals during the oxygenation of sediments in Lake Poyang, China. Water Res. 202, 117442.
Du, H.Y., Chen, C.M., Yu, G.H., Polizzotto, M.L., Sun, F.S., Kuzyakov, Y., 2020. An iron-dependent burst of hydroxyl radicals stimulates straw decomposition and CO_2 emission from soil hotspots: consequences of Fenton or Fenton-like reactions. Geoderma 375, 114512.
Du, H.Y., Yu, G.H., Sun, F.S., Usman, M., Goodman, B.A., Ran, W., Shen, Q.R., 2019. Iron minerals inhibit the growth of *Pseudomonas brassicacearum* J12 via a free-radical mechanism: implications for soil carbon storage. Biogeosciences 16 (7), 1433–1445.
Emerson, D., Fleming, E.J., McBeth, J.M., 2010. Iron-oxidizing bacteria: an environmental and genomic perspective. Annu. Rev. Microbiol. 64 (1), 561–583.
Faust, J.C., Tessin, A., Fisher, B.J., Zindorf, M., Papadaki, S., Hendry, K.R., Doyle, K.A., Marz, C., 2021. Millennial scale persistence of organic carbon bound to iron in Arctic marine sediments. Nat. Commun. 12 (1), 275.
Fischer, H., Kuzyakov, Y., 2010. Sorption, microbial uptake and decomposition of acetate in soil: transformations revealed by position-specific ^{14}C labeling. Soil Biol. Biochem. 42 (2), 186–192.
Flemming, H.C., Wingender, J., Szewzyk, U., Steinberg, P., Rice, S.A., Kjelleberg, S., 2016. Biofilms: an emergent form of bacterial life. Nat. Rev. Microbiol. 14 (9), 563–575.
Garrido-Ramírez, E.G., Theng, B.K.G., Mora, M.L., 2010. Clays and oxide minerals as catalysts and nanocatalysts in Fenton-like reactions–A review. Appl. Clay Sci. 47 (3–4), 182–192.
Georgiou, C.D., Papapostolou, I., Grintzalis, K., 2008. Superoxide radical detection in cells, tissues, organisms (animals, plants, insects, microorganisms) and soils. Nat. Protoc. 3 (11), 1679–1692.
Georgiou, C.D., Sun, H.J., McKay, C.P., Grintzalis, K., Papapostolou, I., Zisimopoulos, D., Panagiotidis, K., Zhang, G., Koutsopoulou, E., Christidis, G.E., Margiolaki, I., 2015. Evidence for photochemical production of reactive oxygen species in desert soils. Nat. Commun. 6 (1), 7100.
Gordon, J., Holman, R.A., McLeod, J.W., 1953. Further observations on the production of hydrogen peroxide by anaerobic bacteria. J. Pathol. Bacteriol. 66 (2), 527–537.

Grace, J.B., 2006. Structural Equation Modeling and Natural Systems. Cambridge University Press, Cambridge, UK.
Haber, F., Weiss, J., Pope, W.J., 1934. The catalytic decomposition of hydrogen peroxide by iron salts. Proc. R. Soc. Lond. Ser. A 147 (861), 332–351.
Hall, S.J., Silver, W.L., 2013. Iron oxidation stimulates organic matter decomposition in humid tropical forest soils. Glob. Chang. Biol. 19 (9), 2804–2813.
Han, R.X., Lv, J.T., Huang, Z.Q., Zhang, S.H., Zhang, S.Z., 2020. Pathway for the production of hydroxyl radicals during the microbially mediated redox transformation of iron (oxyhydr)oxides. Environ. Sci. Technol. 54 (2), 902–910.
Han, R.X., Lv, J.T., Zhang, S.H., Zhang, S.Z., 2021. Hematite facet-mediated microbial dissimilatory iron reduction and production of reactive oxygen species during aerobic oxidation. Water Res. 195, 116988.
Hayyan, M., Hashim, M.A., AlNashef, I.M., 2016. Superoxide ion: generation and chemical implications. Chem. Rev. 116 (5), 3029–3085.
Hochella, M.F., Mogk, D.W., Ranville, J., Allen, I.C., Luther, G.W., Marr, L.C., McGrail, B. P., Murayama, M., Qafoku, N.P., Rosso, K.M., 2019. Natural, incidental, and engineered nanomaterials and their impacts on the Earth system. Science 363 (6434), eaau8299.
Hori, T., Muller, A., Igarashi, Y., Conrad, R., Friedrich, M.W., 2010. Identification of iron-reducing microorganisms in anoxic rice paddy soil by ^{13}C-acetate probing. ISME J. 4 (2), 267–278.
Hori, T., Noll, M., Igarashi, Y., Friedrich, M.W., Conrad, R., 2007. Identification of acetate-assimilating microorganisms under methanogenic conditions in anoxic rice field soil by comparative stable isotope probing of RNA. Appl. Environ. Microbiol. 73 (1), 101–109.
Jeewani, P.H., Gunina, A., Tao, L., Zhu, Z.K., Kuzyakov, Y., Van Zwieten, L., Guggenberger, G., Shen, C.C., Yu, G.H., Singh, B.P., Pan, S.T., Luo, Y., Xu, J.M., 2020. Rusty sink of rhizodeposits and associated keystone microbiomes. Soil Biol. Biochem. 147, 107840.
Kappler, A., Straub, K.L., 2005. Geomicrobiological cycling of iron. Rev. Mineral. Geochem. 59 (1), 85–108.
Kappler, A., Bryce, C., Mansor, M., Lueder, U., Byrne, J.M., Swanner, E.D., 2021. An evolving view on biogeochemical cycling of iron. Nat. Rev. Microbiol. 19 (6), 360–374.
Kleber, M., Bourg, I.C., Coward, E.K., Hansel, C.M., Myneni, S.C.B., Nunan, N., 2021. Dynamic interactions at the mineral-organic matter interface. Nat. Rev. Earth Environ. 2 (6), 402–421.
Kleber, M., Mikutta, R., Torn, M.S., Jahn, R., 2005. Poorly crystalline mineral phases protect organic matter in acid subsoil horizons. Eur. J. Soil Sci. 2005 (56), 717–725.
Kögel-Knabner, I., Guggenberger, G., Kleber, M., Kandeler, E., Kalbitz, K., Scheu, S., Eusterhues, K., Leinweber, P., 2008. Organo-mineral associations in temperate soils: integrating biology, mineralogy, and organic matter chemistry. J. Plant Nutr. Soil Sci. 171 (1), 61–82.
Kraft, B., Jehmlich, N., Larsen, M., Bristow, L.A., Könneke, M., Thamdrup, B., Canfield, D.E., 2022. Oxygen and nitrogen production by an ammonia-oxidizing archaeon. Science 375 (6576), 97–100.
Kuzyakov, Y., Friedel, J.K., Stahr, K., 2000. Review of mechanisms and quantification of priming effects. Soil Biol. Biochem. 32 (11–12), 1485–1498.
Lal, R., 2004. Soil carbon sequestration impacts on global climate change and food security. Science 304 (5677), 1623–1627.
Lalonde, K., Mucci, A., Ouellet, A., Gelinas, Y., 2012. Preservation of organic matter in sediments promoted by iron. Nature 483 (7388), 198–200.
Learman, D.R., Voelker, B.M., Vazquez-Rodriguez, A.I., Hansel, C.M., 2011. Formation of manganese oxides by bacterially generated superoxide. Nat. Geosci. 4 (2), 95–98.
Lehmann, J., Hansel, C.M., Kaiser, C., Kleber, M., Maher, K., Manzoni, S., Nunan, N., Reichstein, M., Schimel, J.P., Torn, M.S., Wieder, W.R., Kögel-Knabner, I., 2020. Persistence of soil organic carbon caused by functional complexity. Nat. Geosci. 13 (8), 529–534.
Li, L.X., Abe, Y., Nagasawa, Y., Kudo, R., Usui, N., Imai, K., Mashino, T., Mochizuki, M., Miyata, N., 2004. An HPLC assay of hydroxyl radicals by the hydroxylation reaction of terephthalic acid. Biomed. Chromatogr. 18 (7), 470–474.
Lieberman, I., Barker, H.A., 1954. The production of hydrogen peroxide by an obligate anaerobe, *Clostridium kluyveri*. J. Bacteriol. 68 (1), 61–62.
Lovley, D.R., 2006. Bug juice: harvesting electricity with microorganisms. Nat. Rev. Microbiol. 4 (7), 497–508.
Luo, X.S., Qian, H., Wang, L., Han, S., Wen, S.L., Wang, B.R., Huang, Q.Y., Chen, W.L., 2020. Fertilizer types shaped the microbial guilds driving the dissimilatory nitrate reduction to ammonia process in a Ferralic Cambisol. Soil Biol. Biochem. 141, 107677.
Melton, E.D., Swanner, E.D., Behrens, S., Schmidt, C., Kappler, A., 2014. The interplay of microbially mediated and abiotic reactions in the biogeochemical Fe cycle. Nat. Rev. Microbiol. 12 (12), 797–808.
Merino, C., Kuzyakov, Y., Godoy, K., Cornejo, P., Matus, F., 2020. Synergy effect of peroxidase enzymes and Fenton reactions greatly increase the anaerobic oxidation of soil organic matter. Sci. Rep. 10 (1), 11289.
Montes, C., Kapelan, Z., Saldarriaga, J., 2021. Predicting non-deposition sediment transport in sewer pipes using Random forest. Water Res. 189, 116639.
Op De Beeck, M., Troein, C., Peterson, C., Persson, P., Tunlid, A., 2018. Fenton reaction facilitates organic nitrogen acquisition by an ectomycorrhizal fungus. New Phytol. 218 (1), 335–343.
Overland, J.E., Dethloff, K., Francis, J.A., Hall, R.J., Hanna, E., Kim, S.J., Screen, J.A., Shepherd, T.G., Vihma, T., 2016. Nonlinear response of mid-latitude weather to the changing Arctic. Nat. Clim. Chang. 6 (11), 992–999.
Page, S.E., Kling, G.W., Sander, M., Harrold, K.H., Logan, J.R., McNeill, K., Cory, R.M., 2013. Dark formation of hydroxyl radical in Arctic soil and surface waters. Environ. Sci. Technol. 47 (22), 12860–12867.
Paustian, K., Lehmann, J., Ogle, S., Reay, D., Robertson, G.P., Smith, P., 2016. Climate-smart soils. Nature 532 (7597), 49–57.
Peng, Q.A., Shaaban, M., Wu, Y.P., Liu, F., Hu, R.G., Wang, B.Y., 2019. Nitrate dependent Fe-oxidizing bacterial diversity in subtropical soils of China. Catena 176, 181–188.
Pereira, M.C., Oliveira, L.C.A., Murad, E., 2012. Iron oxide catalysts: fenton and Fenton-like reactions-a review. Clay Miner. 47 (3), 285–302.
Petigara, B.R., Blough, N.V., Mignerey, A.C., 2002. Mechanisms of hydrogen peroxide decomposition in soils. Environ. Sci. Technol. 36 (4), 639–645.
Porsch, K., Meier, J., Kleinsteuber, S., Wendt-Potthoff, K., 2009. Importance of different physiological groups of iron reducing microorganisms in an acidic mining lake remediation experiment. Microb. Ecol. 57 (4), 701–717.
Qafoku, O., Kovarik, L., Bowden, M.E., Nakouzi, E., Sheng, A.X., Liu, J., Pearce, C.I., Rosso, K.M., 2020. Nanoscale observations of Fe(II)-induced ferrihydrite transformation. Environ. Sci. Nano 7 (10), 2953–2967.
Qiu, H., Zheng, X., Ge, T., Dorodnikov, M., Chen, X., Hu, Y., Kuzyakov, Y., Wu, J., Su, Y., Zhang, Z., 2017. Weaker priming and mineralisation of low molecular weight organic substances in paddy than in upland soil. Eur. J. Soil Biol. 83, 9–17.
Raiswell, R., 2011. Iron transport from the continents to the open ocean: the aging-rejuvenation cycle. Elements 7 (2), 101–106.
Schermelleh-Engel, K., Moosbrugger, H., Müller, H., 2003. Evaluating the fit of structural equation models: tests of significance and descriptive goodness-of-fit measures. Methods Psychol. Res. 8 (2), 23–74.
Schindler, M., Michel, S., Batcheldor, D., Hochella, M.F., 2019. A nanoscale study of the formation of Fe-(hydr)oxides in a volcanic regolith: implications for the understanding of soil forming processes on Earth and Mars. Geochim. Cosmochim. Acta 264, 43–66.
Schoonen, M.A.A., Cohn, C.A., Roemer, E., Laffers, R., Simon, S.R., O'Riordan, T., 2006. Mineral-induced formation of reactive oxygen species. Rev. Mineral. Geochem. 64 (1), 179–221.
Schwertmann, U., Cornell, R.M., 2008. Iron Oxides in the laboratory: Preparation and Characterization. John Wiley & Sons.
Shi, Z.B., Krom, M.D., Bonneville, S., Baker, A.R., Jickells, T.D., Benning, L.G., 2009. Formation of iron nanoparticles and increase in iron reactivity in mineral dust during simulated cloud processing. Environ. Sci. Technol. 43 (17), 6592–6596.
Smith, A.P., Bond-Lamberty, B., Benscoter, B.W., Tfaily, M.M., Hinkle, C.R., Liu, C.X., Bailey, V.L., 2017. Shifts in pore connectivity from precipitation versus groundwater rewetting increases soil carbon loss after drought. Nat. Commun. 8 (1), 1335.
Sulzberger, B., Austin, A.T., Cory, R.M., Zepp, R.G., Paul, N.D., 2019. Solar UV radiation in a changing world: roles of cryosphere-land-water-atmosphere interfaces in global biogeochemical cycles. Photochem. Photobiol. Sci. 18 (3), 747–774.
Tamaru, Y., Yoshida, M., Eltis, L.D., Goodell, B., 2019. Multiple iron reduction by methoxylated phenolic lignin structures and the generation of reactive oxygen species by lignocellulose surfaces. Int. J. Biol. Macromol. 128, 340–346.
Tong, M., Yuan, S., Ma, S., Jin, M., Liu, D., Cheng, D., Liu, X., Gan, Y., Wang, Y., 2016. Production of abundant hydroxyl radicals from oxygenation of subsurface sediments. Environ. Sci. Technol. 50 (1), 214–221.
Trusiak, A., Treibergs, L.A., Kling, G.W., Cory, R.M., 2018. The role of iron and reactive oxygen species in the production of CO_2 in arctic soil waters. Geochim. Cosmochim. Acta 224, 80–95.
Wan, D., Ma, M.K., Peng, N., Luo, X.S., Chen, W.L., Cai, P., Wu, L.H., Pan, H.B., Chen, J. B., Yu, G.H., Huang, Q.Y., 2021. Effects of long-term fertilization on calcium-associated soil organic carbon: implications for C sequestration in agricultural soils. Sci. Total Environ. 772, 145037.
Wan, D., Ye, T.H., Lu, Y., Chen, W.L., Cai, P., Huang, Q.Y., 2019. Iron oxides selectively stabilize plant-derived polysaccharides and aliphatic compounds in agricultural soils. Eur. J. Soil Sci. 70 (6), 1153–1163.
Wang, B., Lerdau, M., He, Y.L., 2017a. Widespread production of nonmicrobial greenhouse gases in soils. Glob. Chang. Biol. 23 (11), 4472–4482.
Wang, T., Persson, P., Tunlid, A., 2021. A widespread mechanism in ectomycorrhizal fungi to access nitrogen from mineral-associated proteins. Environ. Microbiol. 23 (10), 5837–5849.
Wang, X., Dong, H.L., Zeng, Q., Xia, Q.Y., Zhang, L.M., Zhou, Z.Q., 2017b. Reduced iron-containing clay minerals as antibacterial agents. Environ. Sci. Technol. 51 (13), 7639–7647.
Weber, K.A., Achenbach, L.A., Coates, J.D., 2006a. Microorganisms pumping iron: anaerobic microbial iron oxidation and reduction. Nat. Rev. Microbiol. 4 (10), 752–764.
Weber, K.A., Urrutia, M.M., Churchill, P.F., Kukkadapu, R.K., Roden, E.E., 2006b. Anaerobic redox cycling of iron by freshwater sediment microorganisms. Environ. Microbiol. 8 (1), 100–113.
Wen, Y.L., Xiao, J., Liu, F.F., Goodman, B.A., Li, W., Jia, Z.J., Ran, W., Zhang, R.F., Shen, Q.R., Yu, G.H., 2018. Contrasting effects of inorganic and organic fertilisation regimes on shifts in Fe redox bacterial communities in red soils. Soil Biol. Biochem. 117, 56–67.
Xian, H.Y., Zhu, J.X., Tan, W., Tang, H.M., Liu, P., Zhu, R.L., Liang, X.L., Wei, J.M., He, H.P., Teng, H.H., 2019. The mechanism of defect induced hydroxylation on pyrite surfaces and implications for hydroxyl radical generation in prebiotic chemistry. Geochim. Cosmochim. Acta 244, 163–172.
Xun, W.B., Zhao, J., Xue, C., Zhang, G.S., Ran, W., Wang, B.R., Shen, Q.R., Zhang, R.F., 2016. Significant alteration of soil bacterial communities and organic carbon decomposition by different long-term fertilization management conditions of extremely low-productivity arable soil in South China. Environ. Microbiol. 18 (6), 1907–1917.
Yu, G.H., Chi, Z.L., Kappler, A., Sun, F.S., Liu, C.Q., Teng, H.H., Gadd, G.M., 2020. Fungal nanophase particles catalyze iron transformations for oxidative stress removal and iron acquisition. Curr. Biol. 30 (15), 2943–2950.

Yu, G.H., Xiao, J., Hu, S.J., Polizzotto, M.L., Zhao, F.J., McGrath, S.P., Li, H., Ran, W., Shen, Q.R., 2017. Mineral availability as a key regulator of soil carbon storage. Environ. Sci. Technol. 51 (9), 4960–4969.
Yu, G.H., Kuzyakov, Y., 2021. Fenton chemistry and reactive oxygen species in soil: abiotic mechanisms of biotic processes, controls and consequences for carbon and nutrient cycling. Earth Sci. Rev. 214, 103525.
Yu, G.H., Kuzyakov, Y., Luo, Y., Goodman, B.A., Kappler, A., Liu, F.F., Sun, F.S., 2021. Molybdenum bioavailability and asymbiotic nitrogen fixation in soils are raised by iron (oxyhydr)oxide-mediated free radical production. Environ. Sci. Technol. 55 (21), 14979–14989.
Yuan, M.M., Guo, X., Wu, L.W., Zhang, Y., Xiao, N.J., Ning, D.L., Shi, Z., Zhou, X.S., Wu, L.Y., Yang, Y.F., Tiedje, J.M., Zhou, J.Z., 2021. Climate warming enhances microbial network complexity and stability. Nat. Clim. Chang. 11 (4), 343–348.
Zhang, Y., Tong, M., Yuan, S., Qian, A., Liu, H., 2020. Interplay between iron species transformation and hydroxyl radicals production in soils and sediments during anoxic-oxic cycles. Geoderma 370, 114351.